Published in final edited form as:
Neuroscience. 2011 March 10; 176: 142–151. doi:10.1016/j.neuroscience.2010.12.010.

Cuneate and Spinal Trigeminal Nucleus Projections to the Cochlear Nucleus are Differentially Associated with Vesicular Glutamate Transporter-2

Chunhua Zeng[1], **Hersh Shroff**[1], and **Susan Shore**[1,2]

[1]Kresge Hearing Research Institute, Department of Otolaryngology, University of Michigan, Ann Arbor, 48109 USA

[2]Department of Molecular and Integrative Physiology, University of Michigan, Ann Arbor, 48109 USA

Abstract

There are distinct distributions and associations with vesicular glutamate transporters (VGLUTs) for auditory nerve and specific somatosensory projections in the cochlear nucleus. Auditory nerve fibers project primarily to the magnocellular areas of the ventral cochlear nucleus and deepest layer of the dorsal cochlear nucleus and predominantly colabel with VGLUT1; whereas the spinal trigeminal nucleus (Sp5) projections terminate primarily in the granule cell domains (GCD) of CN and predominantly colabel with VGLUT2. Here, we demonstrate that the terminals of another somatosensory pathway, originating in the cuneate nucleus (Cu), also colabel with VGLUT2. Cu projections in cochlear nucleus exhibited a bilateral distribution pattern with ipsilateral dominance, with 30% of these classified as putative mossy fibers (MFs) and 70% as small boutons (SBs). Cu anterograde endings had a more prominent distribution in the GCD than Sp5, with a higher percentage of MF terminals throughout the CN and higher MF/SB ratio in GCD. 56% of Cu endings and only 25% of Sp5 endings colabeled with VGLUT2. In both cases these were mostly MFs with only 43% of Cu SBs and 18% of Sp5 SBs colabeled with VGLUT2. The few Cu and Sp5 terminals that colabeled with VGLUT1 (11% vs. 1%), were evenly distributed between MFs and SBs. The high number of VGLUT2-positive Cu MFs predominantly located in the GCD, may reflect a faster-acting pathway that activates primarily dorsal cochlear nucleus cells via granule cell axons. In contrast, the higher percentage of Sp5-labeled SB terminals and a greater number of projections outside the GCD suggest a slower-acting pathway that activates both dorsal and ventral cochlear nucleus principal cells. Both projections, with their associations to VGLUT2 likely play a role in the enhancement of VGLUT2 after unilateral deafness (Zeng et al., 2009) that may be associated with tinnitus.

Keywords

VGLUTs; cuneate nucleus; spinal trigeminal nucleus; cochlear nucleus; tinnitus

Correspondence to: S. E. Shore, Ph.D., Kresge Hearing Research Institute, 1150 W. Medical Center Drive, Room 5434A Med Sci I, Ann Arbor, MI 48109-5616, sushore@umich.edu, Telephone: (734) 647-2116, Fax: (734) 764-0014.

1. Introduction

The cochlear nucleus (CN) is the first central auditory nucleus receiving inputs from not only the receptor cells of the cochlea via the auditory nerve, but also from a number of somatosensory nuclei, including the spinal trigeminal nucleus (Sp5), trigeminal ganglion and cuneate nucleus (Cu) (Haenggeli et al. 2005, Itoh et al., 1987; Zhou and Shore, 2004; Shore et al., 2000; Weinberg and Rustioni, 1987). These somatosensory inputs are ultimately conveyed to CN principal cells and are involved in multimodal integration with auditory nerve projections to these cells (Zhan and Ryugo, 2007; Zhou and Shore, 2004; Shore, 2005). These non-auditory projections are mostly confined to the granule cell domain (GCD) of the CN (Zhou et al., 2007; Zhan and Ryugo, 2007), which includes both the superficial shell region of the ventral CN (VCN) and the fusiform cell layer of dorsal cochlear nucleus (DCN) and contains numerous small cells, including granule cells (Mugnaini et al., 1980a and 1980b; Hackney et al., 1990; Weedman et al., 1996; Zhou and Shore, 2004).

The cuneate and gracile nuclei together form the dorsal column nuclei, which receive somatosensory inputs from dorsal root ganglion cells that innervate touch, vibratory, and proprioceptive receptors on the body surface (Itoh et al., 1987; Weinberg and Rustioni, 1987; Weinberg and Rustioni, 1989, Young et al., 1995). The projection from the Sp5 to the CN, on the other hand, conveys information about touch, vibration and proprioception from receptors in and around the vocal tract (Haenggeli et al., 2005; Shore and Zhou, 2006). Both the dorsal column and Sp5 pathways are involved in multimodal information processing at an early stage in the auditory pathway, but the types and distributions of terminal projections of the Cu versus Sp5 pathways in the CN remain unclear, thus the specific functional significance of each pathway is yet to be unraveled.

Vesicular glutamate transporters (VGLUTs) package glutamate into synaptic vesicles and serve as excellent markers of glutamatergic projections. The subtypes VGLUT1 and VGLUT2 have distinct distributions in the CN (Fremeau et al., 2001; Herzog et al., 2001; Takamori et al., 2001; Kaneko et al., 2002) and the distinct distributions of auditory and non-auditory projections to the CN are associated with specific VGLUTS. Auditory nerve fibers, which project primarily to the magnocellular areas of the ventral cochlear nucleus (VCNm) and deep layer of the dorsal cochlear nucleus (DCN3) (Brown et al., 1990) exclusively colabel with VGLUT1; whereas spinal trigeminal nucleus (Sp5) projections predominantly colabel with VGLUT2 (Zhou et al., 2007; Zeng et al., 2009). Gómez-Nieto and Rubio (2009) have also shown that VGLUT2- labeled endings of unknown origin contact the dendrites of bushy cells in the rat GCD region.

Although there are indications that the cuneo-cochlear nucleus pathway is glutamatregic (Wright and Ryugo, 1996), the VGLUT transporter involved in this pathway is still unknown. This is particularly important in light of recent findings that VGLUT2 density (Zhou et al., 2007) is increased after unilateral deafness, while VGLUT1, associated with auditory nerve fibers, is decreased (Zeng et al. 2009). This implies that projections that co-label with VGLUT2 are enhanced following deafness. Until now, only the Sp5 endings have been shown to co-label with VGLUT2.

The aim of this study was to determine whether Cu projections to CN, like those from Sp5, co-label with VGLUT2. Furthermore, we wished to compare the distributions and types of endings from each projection site to help elucidate the differential functions of each pathway. By using anterograde tract-tracing methods combined with VGLUT immunohistochemistry, the present study examined the differential distributions of terminals from Cu and Sp5 to the CN in guinea pigs and their association with VGLUT isotypes.

2. Experimental Procedures

2.1. Animal preparation

Seven female pigmented guinea pigs with normal Preyer's reflexes (250–350g, Elm Hill Breeding Labs, Chelmsford, MA) were used in this study. All animals were anesthetized with intramuscular injections of ketamine hydrochloride (Ketaset; 80 mg/Kg) and xylazine (Rompun; 4 mg/Kg) and placed in a stereotaxic frame (David Kopf, Tujunga, CA). Rectal temperature was monitored and maintained at 38±0.5°C with a thermostatically controlled heating pad. Lidocaine was infiltrated around the surgical area of the scalp, and a longitudinal incision was made after the animal was areflexic to a paw pinch and had no corneal reflex. All procedures were carried out in accordance with NIH guidelines for the care and use of laboratory animals (NIH publication No. 80-23), and guidelines provided by the University of Michigan (UCUCA protocol # 08539).

Four guinea pigs were used to identify the locations of labeled terminals from the Cu. Two of these were used to identify the colocalization of VGLUT1-ir and VGLUT2-ir with anterograde terminals from the Cu. Similarly, three guinea pigs were used to identify the locations of labeled terminals from the Sp5, two of which were used for VGLUT colocalization. The surgical procedure for injections of anterograde tracers in Sp5 has been described previously (Zhou and Shore, 2004). The procedure for Cu injections was similar. An opening just lateral-caudal to lambda was drilled in the occipital bone. A Hamilton microsyringe equipped with a glass micropipette (20–30 μm tip) was positioned into the left cuneate nucleus using stereotaxic coordinates (1.8 mm lateral to the midline, 3 mm caudal to the posterior edge of transverse sinus, and 8.8 mm ventral to the surface of the dura). A total volume of 0.1 μl anterograde tracer [10% biotinylated dextran-amine (BDA), MW 10,000, Molecular Probes] was pressure-injected into the Cu. After removing the pipette, the animals were sutured and allowed to recover for six or seven days before being euthanized with FatalPlus (Vortech Pharmaceuticals, Dearborn, MI; 5mg/kg, intraperitoneally) and perfused transcardially with 100 ml of 0.1 M phosphate-buffered saline (PBS; pH 7.4), followed by 400 ml of 4% paraformaldehyde in the same buffer. The brains were isolated and postfixed for 2 hours at 4°C, then transferred into 20% sucrose in 0.1 M phosphate buffer overnight at 4°C. The brainstems were processed as described below for anterograde labeling.

2.2. Tissue processing and immunocytochemistry

The brainstems were sectioned with a freezing microtome at a thickness of 40 μm. Alternate sections were mounted in serial order on clean glass slides and air dried, yielding four equal series. One series was used for labeling BDA and VGLUT1, one was used for BDA and VGLUT2, and one was used for BDA only labeling to check the distribution of projection terminals in CN. To visualize BDA-labeled Sp5 and Cu terminals colabeled with VGLUT-ir, sections were incubated for 2 hours with Cy2 conjugated with streptoavidin (1:300, Jackson ImmunoResearch), followed by immunolabeling with VGLUT1 and VGLUT2.

The VGLUT1 and VGLUT2 immunocytochemistry procedure has been described previously (Zeng, et al., 2009). Briefly, all tissue processing was done at room temperature (20–22°C). Sections were incubated for 30 minutes in a blocking solution containing 1% normal goat serum in 0.1M PBS with 0.1% Triton X-100, PH 7.4, followed by overnight incubation with primary antibodies, VGLUT1 (polyclonal antibody, generated in rabbit, diluted in 1:1000, Synaptic Systems, Germany, Cat. #135 303) or VGLUT2 (polyclonal antibody, generated in rabbit, diluted in 1:1000, Synaptic Systems, Germany, Cat. #135 403). After thoroughly rinsing in PBS, sections were reacted with the secondary antibody (Alexa Fluor 555-conjucated goat anti-rabbit; Invitrogen) for 2 hours. After rinsing, slides

were dehydrated in graded ethanol, then coverslipped using micro-cover gel (Micron Diagnostics, USA). Negative controls were conducted on sections that were not treated with either primary or secondary antibodies, resulting in no immunolabeling. VGLUT antibodies were pre-incubated with corresponding synthetic peptides resulting in negative immunolabeling. (Strep-Tag® fusion protein containing amino acid residues 456 – 560 of rat VGLUT, Cat. #. 135-3P, and Strep-Tag® fusion protein containing amino acid residues 510 – 582 of rat VGLUT2, Cat. #135-4P, Synaptic Systems, Germany). Western blots previously performed (Zhou et al., 2007) demonstrated anti-VGLUT1 antibody with a single band at ~ 60 kDa on protein extracted from both CN and cerebellum and anti-VGLUT2 antibody as a single band at ~65 kDa, corresponding to the molecular weights predicted for VGLUT1 and VGLUT2, respectively. Positive controls for VGLUT-ir were performed in the cerebellar cortex (Hioki et al., 2003; Kaneko et al., 2002; Takamori et al., 2001).

2.3. Image processing and analysis of anterograde projection data

Sections were examined with a fluorescent microscope equipped with the appropriate filters for Alexa fluoro 555 and Cy2 (Leica, DM). The brightest BDA injection areas in Cu or Sp5 were determined and represented the injection site. Only guinea pigs with injection sites restricted to the confines of Cu or Sp5 were included in this report (4 for restricted Cu injections, 3 for restricted Sp5 injections). The locations of all seven injection sites are summarized in a serial brainstem template, as shown in Figure 1 (Freehand, Macromedia, Inc). One Cu injection site (64898-2-Cu) was photographed across serial sections which are presented in Figure 2.

Under epifluorescence, the labeled Cu and Sp5 terminals in both CN were manually counted on every section in each group. The quantification was based on terminals in both CN unless otherwise stated. The Cu and Sp5 terminal endings were further classified as: 1) mossy fiber-like terminal endings (MF): large irregular swellings (≥2.5 μm), which usually give rise to collaterals; or 2) small boutons (SB): small and round or oval (<2.5 μm), including en passant and terminal boutons (Zhou and Shore, 2004). Double labeling of Cu and Sp5 terminals with VGLUT-ir were determined by frequently switching the filters and adjusting the focus of the objective lens. Colocalization was established when the two different labels (red and green) exactly marked the same profile at the same focusing level. In some cases, double-labeled immunofluorescent terminals were also identified by confocal laser microscopy (Olympus 500). The method of identifying double-labeled Cu / Sp5 – VGLUT1 / VGLUT2 terminals in the CN corresponded well with the confocal findings. So, for either Cu or Sp5 terminals, there were 4 categories: 1) SB-non-colabeled with VGLUT1/ VGLUT2; 2) SB-colabeled with VGLUT1/VGLUT2; 3) MF-non-colabeled with VGLUT1/ VGLUT2; 4) MF-colabeled with VGLUT1/VGLUT2. The number of terminal counts was multiplied by 4 to achieve the total terminal counts and corrected for double counting errors by using Abecrombie's correction: corrected number = count × [section thickness/ (section thickness + terminal size)] (Abercrombie, 1946). Chi square test and t-test were used for statistical analysis.

3. RESULTS

3.1. The distribution of Cu anterograde labeling in CN

Results presented here are derived from 4 guinea pigs with restricted injections in Cu, and are compared with 3 guinea pigs with restricted injections in Sp5. The locations of all six injection sites are summarized in a serial brainstem template, as shown in Figure 1. One Cu injection site (64898-2-Cu), photographed across serial sections, is shown in Figure 2. Of the 4 Cu injections, two were in the caudal part of Cu and two were in the rostral part of Cu. Cu injections did not result in any retrograde labeling in either CN.

Ipsilateral projections from one Cu injection (7-1-2008-Cu) and one Sp5 injection (64898-5-Sp5) were mapped on a brainstem template (Figure 3) for visual comparison. The Cu anterograde projections in CN were bilateral with ipsilateral dominance. Labeled puncta were located mostly in the GCD (grey zone in Figure 3, left column). Some puncta were found in the deep layers of DCN (DCN3), and a few puncta were sparsely located in magnocellular regions of PVCN and AVCN. Some labeled fibers were found in the molecular cell layer (DCN1), but no puncta were observed in this region. Labeled Cu terminals were either large, irregular MFs or small, en passant boutons (see below).

The total number of projection terminals observed after Cu injections was considerably less than from the Sp5 injections. The terminal distribution pattern from each nucleus was also different (Figure 3 and Figure 4a). The terminal distribution of the Cu projection was bilateral with ipsilateral dominance, with an average of 65% of endings in ipsilateral CN versus 35% in contralateral CN. Sp5-labeled terminals had 86% ipsilateral, with only 14% in contralateral CN. While numerous Cu-labeled and Sp5-labeled terminals were found predominantly in the GCD, Cu projections exhibited a higher percentage of terminals in the GCD (80%), compared to the projections from Sp5 (56%, $P<0.05$, Figure 4b). In contrast, many Sp5-labeled terminals were also found in the magnocellular regions of VCN (Figure 4a).

3.2. Morphology of endings

Both Sp5- and Cu- labeled terminals were of two types (Figure 4): large, irregular MFs or small, en passant boutons (Figure 5). However, the percentages of these types differed for each projection: 32% of Cu-labeled terminals were MFs, almost all (98%) confined to the GCD where the MFs-to-SB ratio was 1:1.5; 68% of Cu-labeled terminals were SBs. In contrast, only 10% of Sp5-labeled terminals in CN were MFs also mostly confined to the GCD (96 %) with a MFs-to-SB ratio of 1:5. The remaining 90% were SBs (Figures 4a, 4b). The terminals located in the magnocellular regions (AVCN and PVCN) were exclusively SBs for both Cu and Sp5 projections. Although MFs were almost exclusively found in the GCD for both Cu and Sp5 projections, 69% of Cu-labeled SBs and 55% of Sp5-labeled SBs were also located in the GCD. Thus, Cu anterograde endings had a predominant distribution in GCD, with most MFs in GCD, and a higher MF/SB ratio in the GCD ($P<0.001$) than for Sp5. Sp5 projections had more terminals outside of the GCD than Cu projections and a greater number of SBs reflecting this distribution.

3.3. Colocalization of Cu endings with VGLUT2

We have previously shown that Sp5 terminals in CN colabel with VGLUT2 (Zhou et al., 2007), thus in the present study, we examined the VGLUT expression and its association with Cu terminals in CN (N=2) and compared them with Sp5 colocalization (N=2). Cu-labeled terminal endings that were colocalized with VGLUT2 were either MFs or SBs (Figure 6), mostly located in the GCD (96%) with a small percentage in DCN3 and AVCN (Figure 7), whereas VGLUT2 positive Sp5 endings, although also predominant in the GCD (83%) had some colabeled endings in DCN3 and PVCN.

Although both double-labeled Cu- and Sp5- puncta were predominant in GCD, a much higher percentages (56%) of Cu terminals throughout CN colabeled with VGLUT2, compared with only 25% for Sp5 ($p<0.001$). In the GCD, the main recipient area of both Sp5 and Cu terminals, more Cu endings colabeled with VGLUT2 than SP5 (66% vs. 33%, $p<0.001$).

Cu endings that colabeled with VGLUT2 showed morphological differences from Sp5 endings that colabeled with VGLUT2 (Figure 7). 86% of Cu MFs throughout the CN

colabeled with VGLUT2, which was similar to Sp5 MFs (85%, $p>0.05$). In contrast, 43% of Cu SBs terminals colabeled with VGLUT2, a much higher percentage than was evident for Sp5 SB terminals (18%, $p<0.001$).

3.4. Colocalization of Cu endings with VGLUT1

In contrast to VGLUT2, only 11% of total Cu endings colabeled with VGLUT1, significantly fewer than were colabeled with VGLUT2 (56%, $p<0.001$). Cu endings that were colabeled with VGLUT1 were located only in the GCD and DCN3 (Figure 8), and were significantly more frequent than VGLUT1 positive Sp5 endings, which were also confined to the GCD (1%, $p<0.001$) (Figure 9).

VGLUT1-positive Cu endings were not morphologically different from those that did not colabel with VGLUT1. 12% of Cu MFs and 11% of Cu SBs terminals throughout the CN colabeled with VGLUT1, whereas 4% of Sp5 MFs and 1% of SBs terminals were VGLUT1 positive (12% vs. 4%, $p<0.01$; 11% vs. 1%, $p<0.001$).

4. Discussion

Since the four Cu injections in this study were entirely contained within the boundaries of the nucleus, these anterograde projections are representative of the pathway from Cu to CN. Because our injections were confined to the middle and deep core regions of Cu, we could not confirm findings by a previous retrograde tracing study in the rat that the lateral edge of the Cu was the main site of origin of the projection neurons (Weinberg and Rustioni, 1987).

The results of this anterograde tract-tracing study in guinea pig demonstrate a bilateral projection from the Cu to the CN, with a major component to the ipsilateral CN, consistent with earlier findings in rat (Weinberg and Rustioni, 1987) and in cat (Itoh et al., 1987). Like previous findings in the rat (Wright and Ryugo, 1996), Cu terminal endings in guinea pig were either large, irregular claw-like MFs that were previously shown to contain numerous round synaptic vesicles (Mugnaini et al., 1980b), or SBs. Almost all of the MFs (98%) and a smaller percentage (69%) of the SBs were confined to the GCD, confirming that this region is the main recipient of the somatosensory inputs from the Cu. Other sources of MF and SB input to the GCD are the lateral reticular nucleus, the pontine nuclei and inferior olive (Weinberg and Rustioni, 1987; Zhou and Shore, 2004; Ryugo et al., 2003), as well as the contralateral CN (Zhou et al., 2010). In this study we compared the distributions and types of endings from Cu and Sp5 with the intention of discovering differences in distributions of MFs versus SBs that would give us clues as to the differential functions of each pathway. For example, if Cu endings were mostly MFs this would imply a faster-acting pathway than one comprised mainly of SBs. This is due to the high Na^{+}-channel density in MF boutons and fast gating of presynaptic Ca^{++} channels, which produce a large and brief presynaptic Ca^{++} influx, triggering transmitter release with a high degree of temporal precision (McBain, 2008). It turns out that the major difference between these pathways is that there are more MFs in the GCD from the Cu pathway than the Sp5 pathway, the latter also projecting to magnocellular VCN. This suggests that the Cu pathway may be a faster-acting pathway that predominantly activates neurons in the DCN via the granule cell axons, the parallel fibers. On the other hand, the Sp5 pathway may be slower (comprised of more SBs) and activates principal neurons in both the VCN and DCN.

The functional roles of MF endings in the CN are not well understood. However in the hippocampus, individual dentate granule cells give rise to MFs that have three types of target-specific presynaptic terminals - large mossy terminals (4–10 μm in diameter), filopodial extensions (0.5–2.0 μm) projecting from the large mossy boutons, and small en passant varicosities (0.5–2.0 μm) (McBain, 2008). Electrophysiological studies have shown

that the large and small synaptic specializations are functionally distinct and that the balance of excitation and inhibition within the CA3 region of the hippocampus shifts depending on the firing rate of the dentate granule cells (for review see McBain, 2008). Moreover, due to the high Na^{+}-channel density in MF boutons and fast gating of presynaptic Ca^{++} channels, there is a large and brief presynaptic Ca^{++} influx, which triggers transmitter release with a high degree of temporal precision. Thus, there are differential mechanisms of transmission and both short and long-term plasticity (Chen et al., 2010) at MF synapses in the hippocampus. Whether MF terminals in the CN display similar properties remains to be determined, but they are likely to be involved in the synaptic plasticity previously demonstrated in the CN (Tzounopoulos et al., 2004; 2007).

Both Cu and Sp5 projections to CN showed more SB terminals than MFs (68% vs. 32%, 90% vs. 10%). However, in contrast to the MFs, which were almost exclusively located in the GCD for both Cu and Sp5 projections, the majority (69 %) of Cu-labeled SBs and half of Sp5-labeled SBs were located in the GCD. It is unclear how these numerous SBs contribute to coding in the CN, but they almost certainly make contacts with cells other than granule cells (Haenggeli et al., 2005; Zhou and Shore, 2004, Zhou et al., 2007; Wright and Ryugo, 1996). More investigation into the types of cells they innervate is needed to elucidate the SBs functional significance.

The colocalization of VGLUT2 with Cu terminals in the CN shown in this study confirms that the Cu pathway to the CN is glutamatergic and demonstrates that Cu projections, like those from Sp5 and the contralateral CN (Zhou et al., 2010) use VGLUT2 to mediate glutamate transport at both MF and SB terminal endings. More than half of all Cu-labeled MF and SB terminals colabeled with VGLUT2, and were highly restricted to the GCD. The Cu-CN pathway showed more VGLUT2 labeling than the Sp5 pathway.

By activating the granule cells, which excite both pyramidal cells and their inhibitory interneurons, the cartwheel cells in the DCN (Davis and Young, 1997), the Cu and Sp5 projections mediate both excitation and inhibition to the principal output neurons of the CN, the pyramidal cells. Thus, some pyramidal cells may be less or more responsive to auditory stimulation when the somatosensory pathways are activated. It is still unknown how this balance is achieved but the GCD plays an important role in integrating the auditory and non-auditory information. Since Cu receives direct primary inputs from dorsal root ganglion cells that innervate touch, vibratory and proprioceptive receptors in the head and neck, the MFs from Cu have been hypothesized to provide proprioceptive information related to pinna and head position (Young et al., 1995), and may play an important role in head orientation for the purpose of pursing the sound source (Wright and Ryugo, 1996; Kanold and Young, 2001).

The projections from Sp5 to CN, on the other hand, originate in regions that represent vocalization (Luthe et al., 2000) and may therefore mediate the suppression of body-generated sounds such as chewing and respiration (Shore and Zhou, 2006; Shore, 2005; Haenggeli et al., 2005). The Sp5 projections to CN display a broader terminal distribution across the CN, with more Sp5-labeled terminal endings located outside the GCD, and a smaller MF/SB ratio in all Sp5-labeled regions. However, Sp5 projections to the CN still showed a predominant MF distribution within the GCD. This indicates that MFs are an important component in the somatosensory-granule cell interneuron circuit of the cochlear nucleus, mediating the integration between auditory nerve inputs and the somatosensory inputs from Sp5 and the Cu. The higher MF contribution to Cu projections than Sp5 projections to CN may indicate these two somatosensory nuclei have different roles in multimodal integration, one (Cu) more involved with temporal precision and neural

plasticity and the other (Sp5) perhaps having a slower, modulatory function that involves neurons in the VCN as well as the DCN.

Both dorsal column and trigeminal system inputs to the CN are implicated in the pathophysiology of tinnitus, or phantom sounds. Many subjects with this disorder are able to modulate the loudness or pitch of their tinnitus with somatic manipulations of their face, head, neck, shoulders or arms, suggesting that trigeminal and/or dorsal column inputs to the auditory system play a role in the pathophysiology of tinnitus (Herraiz et al., 2007; Levine, 1999; Pinchoff et al., 1998). The findings of the present study confirm and extend previous findings that this interaction begins at the lowest level of the auditory nervous system, the cochlear nucleus. The bilateral nature of the innervation, with ipsilateral predominance, from both Cu and Sp5 suggest that these manipulations should be more effective for same-side modulations of tinnitus, consistent with reports in the literature. However, the bilateral distribution also suggests that bilateral modulations should also be possible. In addition, since we have previously shown that VGLUT2 density is increased after unilateral deafness, while VGLUT1, associated with auditory nerve fibers, is decreased (Zeng et al., 2009), indicating that projections that co-label with VGLUT2 are enhanced following deafness. Here we demonstrate that projections from Cu as well as from Sp5 and the contralateral CN (Zhou et al, 2010) may may contribute to the enhancement of VGLUT2 observed after deafferentation and perhaps play a role in the modulation and generation of tinnitus (Dehmel et al., 2008; Levine et al., 2007). Knowledge of the distributions and functional significance of these two pathways could therefore contribute to the development of therapies for tinnitus involving selective electrical stimulation or targeted pharmacological treatments.

Research Highlights

- Cuneate projections to the CN terminate as mossy fibers or small boutons
- Cuneate projections to the CN co-label with VGLUT2
- Trigeminal projections distribute more widely in CN than cuneate projections
- Cuneate and trigeminal projections to CN label almost exclusively with VGLUT2
- Few terminals from Cuneate and Trigeminal Nuclei in CN label with VGLUT1

Acknowledgments

We thank Sanford Bledsoe for critical reading of the manuscript and Yilei Cui for contributing an injection site to the study. This work was supported by NIH R01 DC004825 and P30 05188.

References

Abercrombie M. Estimation of nuclear population from microtome sections. Anatomical Record 1946;94:239–247. [PubMed: 21015608]

Brown MC, Ledwith JV 3rd. Projections of thin (type-II) and thick (type-I) auditory-nerve fibers into the cochlear nucleus of the mouse. Hear Res 1990;49:105–118. [PubMed: 1963423]

Chen CC, Yang CH, Huang CC, Hsu KS. Acute stress impairs hippocampal mossy fiber-CA3 long-term potentiation by enhancing cAMP-specific phosphodiesterase 4 activity. Neuropsychopharmacology 2010;35:1605–1617. [PubMed: 20237461]

Davis KA, Young ED. Granule cell activation of complex-spiking neurons in dorsal cochlear nucleus. J Neurosci 1997;17:6798–6806. [PubMed: 9254690]

Dehmel S, Cui YL, Shore SE. Cross-modal interactions of auditory and somatic inputs in the brainstem and midbrain and their imbalance in tinnitus and deafness. Am J Audiol 2008;17:S193–S209. [PubMed: 19056923]

Fremeau RT Jr, Kam K, Qureshi T, Johnson J, Copenhagen DR, Storm-Mathisen J, Chaudhry FA, Nicoll RA, Edwards RH. Vesicular glutamate transporters 1 and 2 target to functionally distinct synaptic release sites. Science 2004;304(5678):1815–1819. [PubMed: 15118123]

Gómez-Nieto R, Rubio ME. A bushy cell network in the rat ventral cochlear nucleus. J Comp Neurol 2009;516:241–263. [PubMed: 19634178]

Hackney CM, Osen KK, Kolston J. Anatomy of the cochlear nuclear complex of guinea pig. Anat Embryol 1990;182:123–149. [PubMed: 2244686]

Haenggeli CA, Pongstaporn T, Doucet JR, Ryugo DK. Projections from the spinal trigeminal nucleus to the cochlear nucleus in the rat. J Comp Neurol 2005;484:191–205. [PubMed: 15736230]

Herraiz C, Toledano A, Diges I. Trans-electrical nerve stimulation (TENS) for somatic tinnitus. Prog Brain Res 2007;166:389–394. [PubMed: 17956803]

Herzog E, Bellenchi GC, Gras C, Bernard V, Ravassard P, Bedet C, Gasnier B, Giros B, El Mestikawy S. The existence of a second vesicular glutamate transporter specifies subpopulations of glutamatergic neurons. Neurosci 2001;21:RC181.

Hioki H, Fujiyama F, Taki K, Tomioka R, Furuta T, Tamamaki N, Kaneko T. Differential distribution of vesicular glutamate transporters in the rat cerebellar cortex. Neuroscience 2003;117:1–6. [PubMed: 12605886]

Itoh K, Kamiya H, Mitani A, Yasui Y, Takada M, Mizuno N. Direct projections from the dorsal column nuclei and the spinal trigeminal nuclei to the cochlear nuclei in the cat. Brain Res 1987;400:145–150. [PubMed: 2434184]

Kaneko T, Fujiyama F, Hioki H. Immunohistochemical localization of candidates for vesicular glutamate transporters in the rat brain. J Comp Neurol 2002;444:39–62. [PubMed: 11835181]

Kanold PO, Young ED. Proprioceptive information from the pinna provides somatosensory input to cat dorsal cochlear nucleus. J Neurosci 2001;21:7848–7858. [PubMed: 11567076]

Levine RA. Somatic (craniocervical) tinnitus and the dorsal cochlear nucleus hypothesis. Am J Otolaryngol 1999;20:351–362. [PubMed: 10609479]

Levine RA, Nam EC, Oron Y, Melcher JR. Evidence for a tinnitus subgroup responsive to somatosensory based treatment modalities. Prog Brain Res 2007;166:195–207. [PubMed: 17956783]

Luthe L, Hausler U, Jurgens U. Neuronal activity in the medulla oblongata during vocalization. A single-unit recording study in the squirrel monkey. Behav Brain Res 2000;116:197–210. [PubMed: 11080551]

McBain CJ. Differential mechanisms of transmission and plasticity at mossy fiber synapses. Prog Brain Res 2008;169:225–240. [PubMed: 18394477]

Mugnaini E, Osen KK, Dahl AL, Friedrich VL Jr, Korte G. Fine structure of granule cells and related interneurons (termed Golgi cells) in the cochlear nuclear complex of cat, rat and mouse. J Neurocytol 1980a;9:537–570. [PubMed: 7441303]

Mugnaini E, Warr WB, Osen KK. Distribution and light microscopic features of granule cells in the cochlear nuclei of cat, rat and mouse. J Comp Neurol 1980b;191:581–606. [PubMed: 6158528]

Pinchoff RJ, Burkard RF, Salvi RJ, Coad ML, Lockwood AH. Modulation of tinnitus by voluntary jaw movements. Am J Otol 1998;19:785–789. [PubMed: 9831155]

Ryugo DK, Haenggeli CA, Doucet JR. Multimodal inputs to the granule cell domain of the cochlear nucleus. Exp Brain Res 2003;153:477–485. [PubMed: 13680048]

Shore SE, Vass Z, Wys NL, Altschuler RA. Trigeminal ganglion innervates the auditory brainstem. J Comp Neurol 2000;419(3):271–285. [PubMed: 10723004]

Shore SE. Multisensory integration in the dorsal cochlear nucleus: unit responses to acoustic and trigeminal ganglion stimulation. Eur J Neurosci 2005;21(12):3334–3348. [PubMed: 16026471]

Shore SE, Zhou J. Somatosensory influence on the cochlear nucleus and beyond. Hear Res 2006;216–217:90–99.

Takamori S, Rhee JS, Rosenmund C, Jahn R. Identification of differentiation-associated brain-specific phosphate transporter as a second vesicular glutamate transporter (VGLUT2). J Neurosci 2001;21:RC182. [PubMed: 11698620]

Tzounopoulos T, Kim Y, Oertel D, Trussell LO. Cell-specific, spike timing-dependent plasticities in the dorsal cochlear nucleus. Nat Neurosci 2004;7:719–725. [PubMed: 15208632]

Tzounopoulos T, Rubio ME, Keen JE, Trussell LO. Coactivation of pre- and postsynaptic signaling mechanisms determines cell-specific spike-timing-dependent plasticity. Neuron 2007;54:291–301. [PubMed: 17442249]

Weedman DL, Pongstaporn T, Ryugo DK. Ultrastructural Study of the Granule Cell Domain of the Cochlear Nucleus in Rats: Mossy Fiber Endings and Their Targets. J Comp Neurol 1996;369:345–360. [PubMed: 8743417]

Weinberg RJ, Rustioni A. A cuneocochlear pathway in the rat. Neuroscience 1987;20:209–219. [PubMed: 3561761]

Weinberg RJ, Rustioni A. Brainstem projections to the rat cuneate nucleus. J Comp Neurol 1989;282:142–156. [PubMed: 2468698]

Wright DD, Ryugo DK. Mossy fiber projections from the cuneate nucleus to the cochlear nucleus in the rat. J Comp Neurol 1996;365:159–172. [PubMed: 8821448]

Young ED, Nelken I, Conley RA. Somatosensory effects on neurons in dorsal cochlear nucleus. J Neurophysiol 1995;73:743–765. [PubMed: 7760132]

Zeng C, Nannapaneni N, Zhou J, Hughes LF, Shore S. Cochlear damage changes the distribution of vesicular glutamate transporters associated with auditory and nonauditory inputs to the cochlear nucleus. J Neurosci 2009;29:4210–4217. [PubMed: 19339615]

Zhan X, Ryugo DK. Projections of the lateral reticular nucleus to the cochlear nucleus in rats. J Comp Neurol 2007;504:583–598. [PubMed: 17701985]

Zhou J, Shore S. Projections from the trigeminal nuclear complex to the cochlear Nuclei: a retrograde and anterograde tracing study in the guinea pig. J Neurosci Res 2004;78:901–907. [PubMed: 15495211]

Zhou J, Nannapaneni N, Shore S. Vessicular glutamate transporters 1 and 2 are differentially associated with auditory nerve and spinal trigeminal inputs to the cochlear nucleus. J Comp Neurol 2007;500:777–787. [PubMed: 17154258]

Zhou J, Zeng C, Cui Y, Shore S. Vesicular Glutamate Transporter 2 Is Associated with the Cochlear Nucleus Commissural Pathway. J Assoc Res Otolaryngol 2010;11:675–687. [PubMed: 20574763]

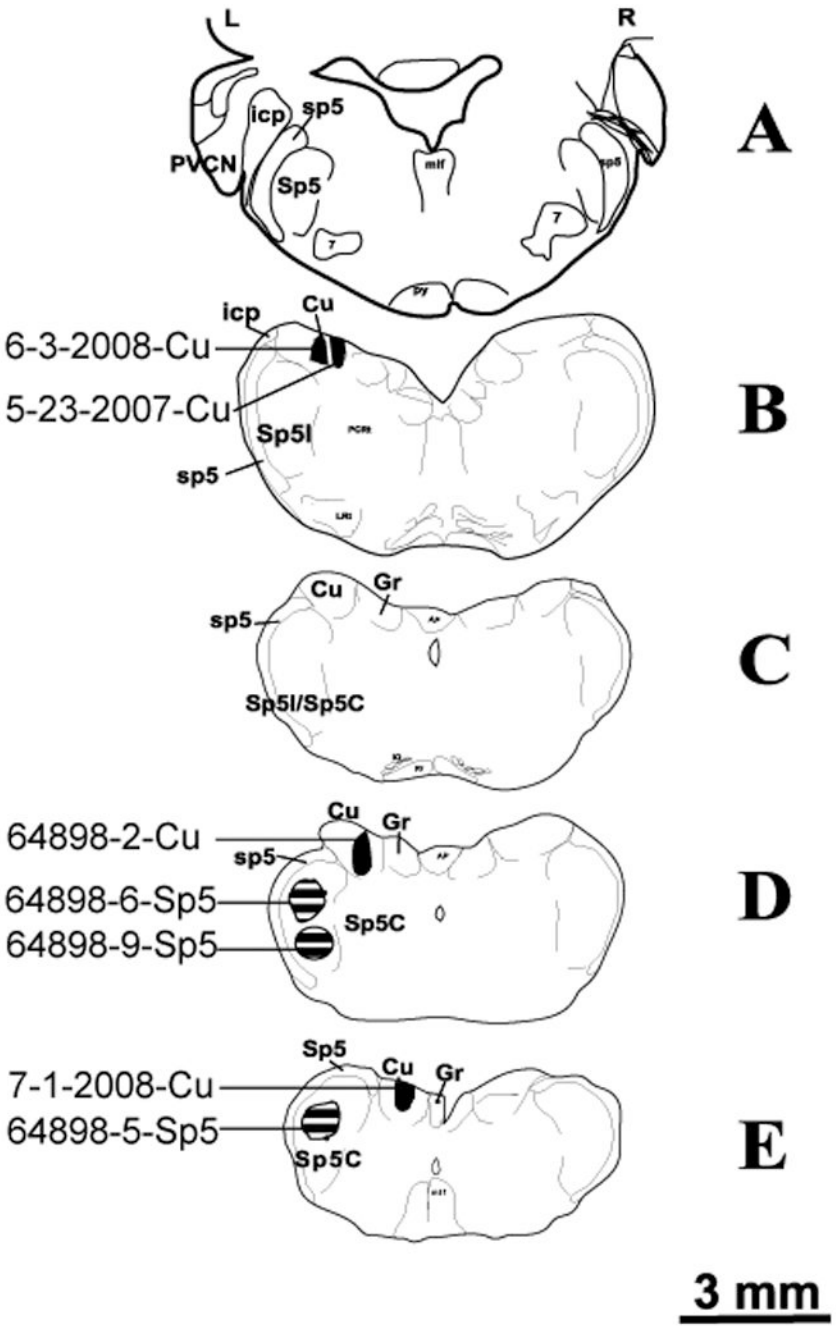

Figure 1.

Drawings of rostral (A)-to-caudal (E) transverse sections of the brain stem. The shaded areas represent four Cu injection sites (solid) and three Sp5 (cross hatched) injection sites. Note all four Cu injections are smaller than the Sp5 injections. Sp5, spinal trigeminal nucleus; sp5, spinal trigeminal tract; SpI, pars interpolaris of Sp5; Sp5C, pars caudalis of Sp5; icp, inferior cerebellar peduncle; Cu, cuneate nucleus; Gr, gracile nucleus; PVCN, posteroventral cochlear nucleus.

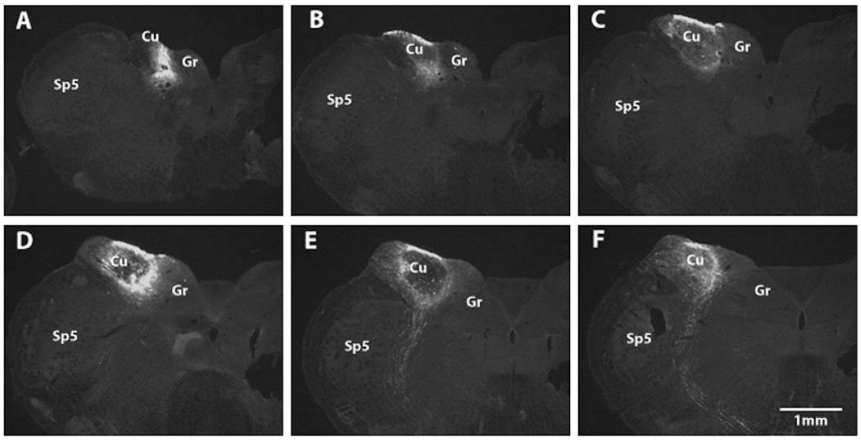

Figure 2.

Photomicrographs of the injection site in guinea pig 64898-2 as shown in transverse brainstem sections after incubation with Cy2 conjugated with streptoavidin. The injection site is restricted to Cu without diffusion to adjacent areas. The sections from A to F are caudal–to-rostral. Sp5, spinal trigeminal nucleus; Cu, cuneate nucleus; Gr, gracile nucleus.

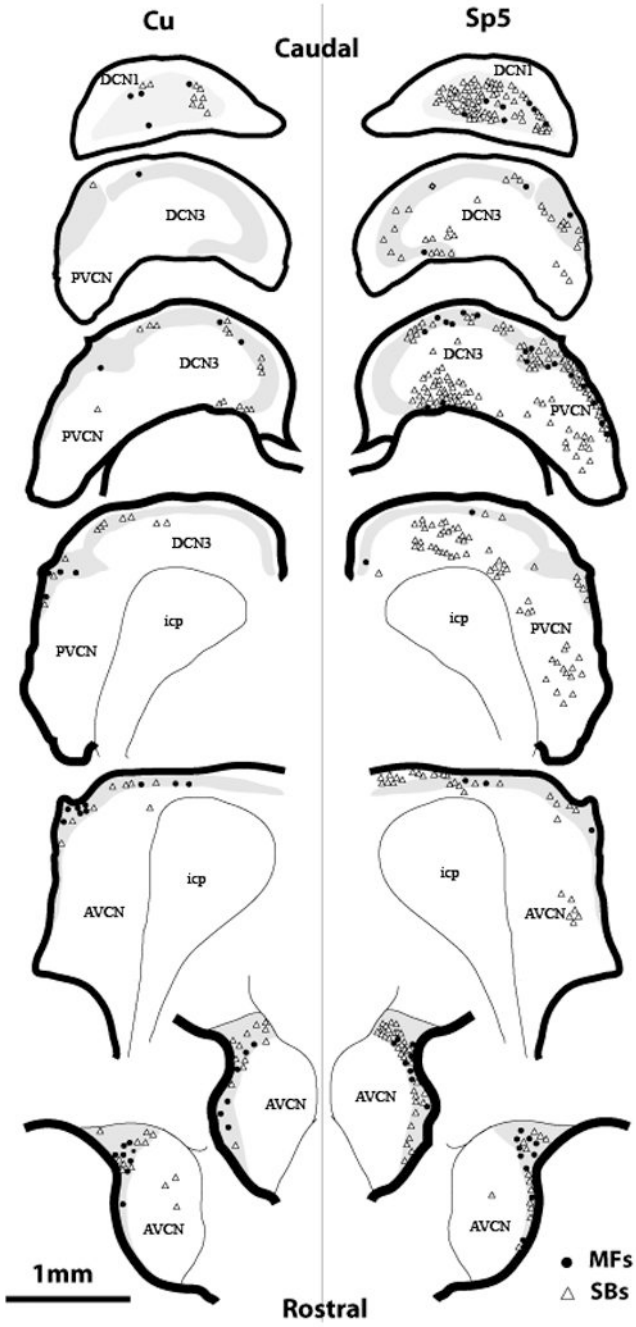

Figure 3.

Reconstruction of anterograde terminal-labeling distributions in ipsilateral CN after one Cu (left column) and one Sp5 injection (Right column). BDA injection sites (7-1-2008-Cu and 64898-5-Sp5) are shown in Figure 1. All dots in left column represent ipsilateral projections, which account for 75% of all anterograde terminal endings after BDA injection in 7-1-2008-Cu; all dots in right column represent ipsilateral projections, which account for 82% of all aterograde terminal endings after BDA injection in 64898-5-Sp5. The grey zones designate GCD. Each dot represents one terminal ending, filled circle = MFs, open triangle = SBs. CN, cochlear nucleus; AVCN, anteroventral CN; PVCN, posteroventral CN; DCN, dorsal CN; icp, inferior cerebellar peduncle.

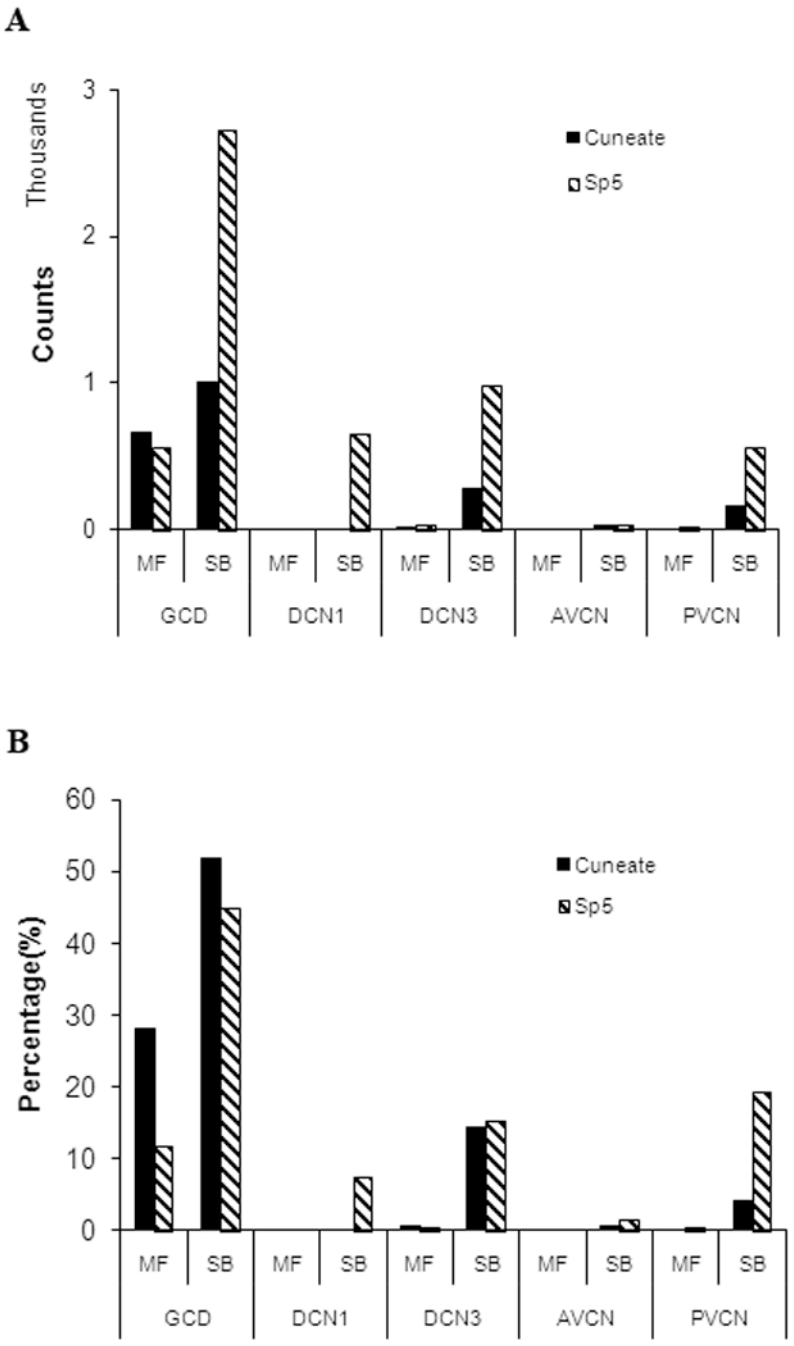

Figure 4.

Counts of labeled Cu- and Sp5-terminal endings in different CN subdivisions (Cu, n=4; Sp5, n=3). A. Cu-labeled endings were much less numerous than Sp5-labeled endings. Both Cu- and Sp5-labeled puncta were found predominantly in the GCD. A considerable number of Sp5- but not Cu-labeled puncta were located in the magnocellular regions of VCN. B. 80% of Cu projections were located in GCD, compared to 56% of Sp5 projections ($P<0.05$). 32% of Cu-labeled terminals were MFs and 98% of MFs were confined to the GCD; In contrast, 10% of Sp5-labeled terminals were MFs with 96% of MFs in GCD. GCD, granular cell domain; DCN3, deep layer of dorsal cochlear nucleus; DCN1, superficial layer of dorsal cochlear nucleus; AVCN, anteroventral CN; PVCN, posteroventral CN.

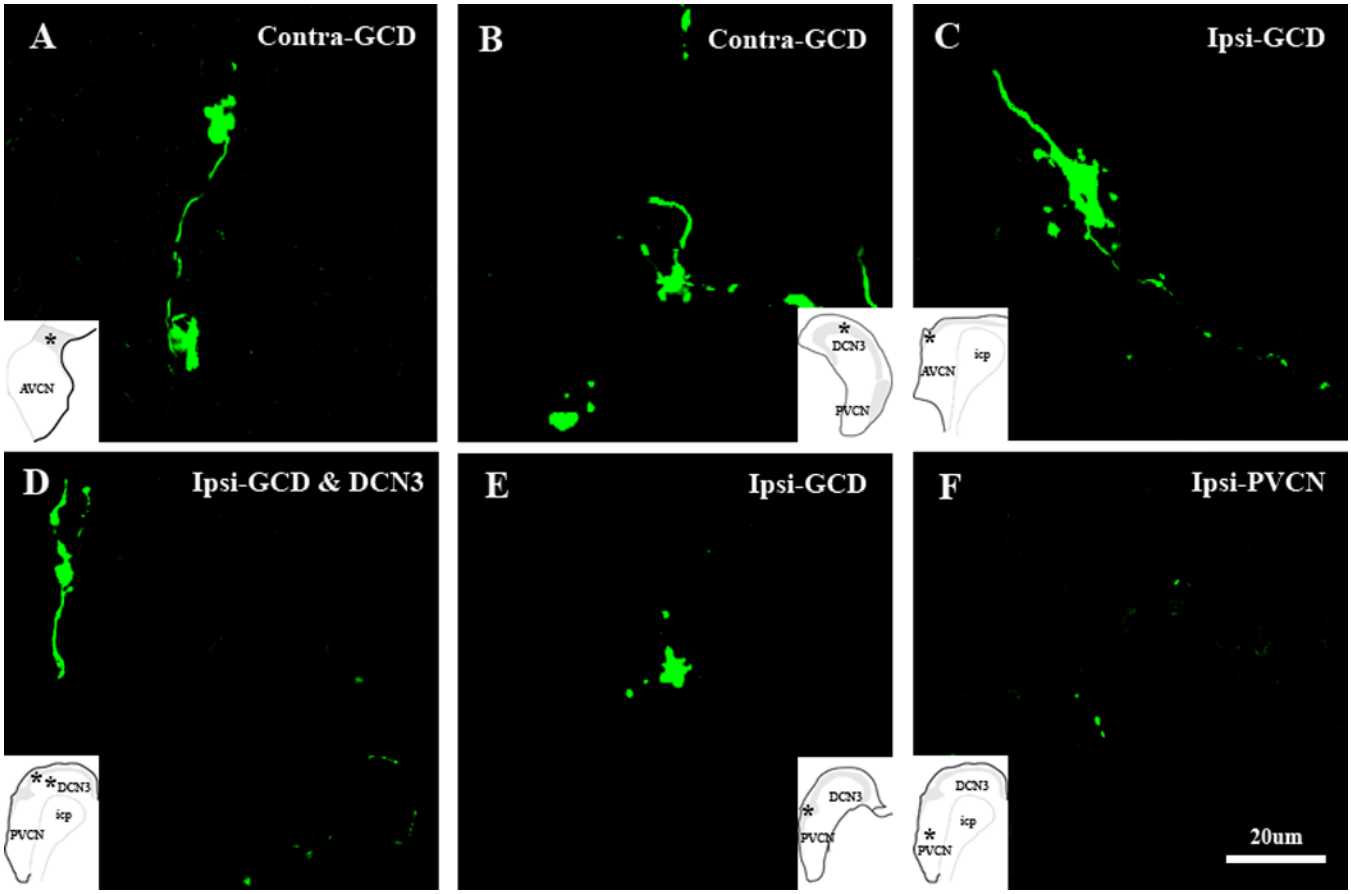

Figure 5.

High-magnification confocal images (×100) showing ipsilateral and contralateral Cu-labeled terminal endings in different regions of the CN, insets in A–F show the terminal locations. A. Cu-labeled MFs in contralateral GCD. B. Cu-labeled MFs in DCN2 of contralateral CN. C–F. Cu-labeled MFs and SBs in ipsilateral CN. C and E show Cu-labeled MFs and SBs in GCD adjacent to AVCN and PVCN, respectively. D. MFs in DCN2 and SBs in DCN3. F. SBs in PVCN.

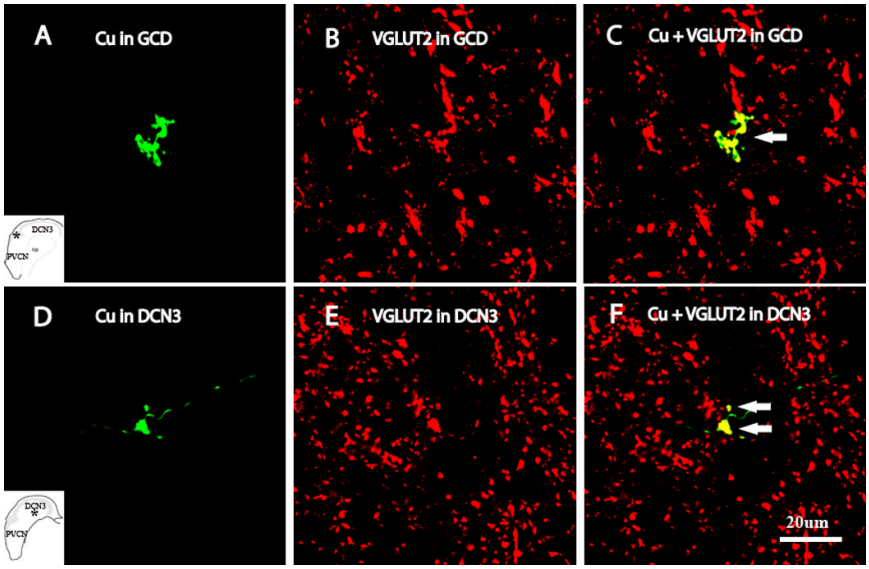

Figure 6.

High-magnification confocal images (×100) showing colocalization of anterogradely-labeled Cu terminal endings with VGLUT2 in different regions of the CN, as designated in the insets by asterisks. A and D show BDA-labeled Cu terminals (green); B and D show VGLUT2 labeling (Red); C and F show double-labled terminals Colocalizations of VGLUT2 with Cu MFs and SB are shown by arrows in C and F.

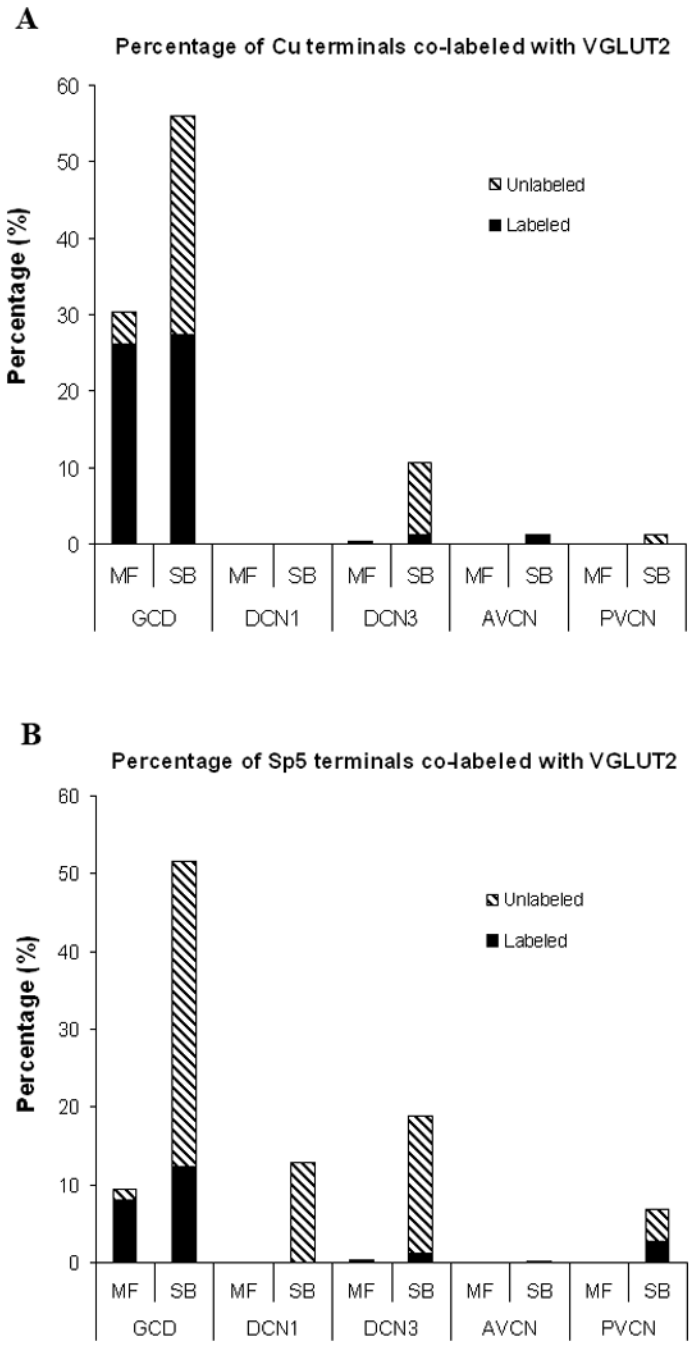

Figure 7.

Counts of labeled Cu and Sp5 terminal endings colocalized with VGLUT2 in different subdivisions of the CN (Cu, n=2; Sp5, n=2). A: Percentage of Cu terminal endings colabeled or not colabeled with VGLUT2. 56% of all Cu terminals colabeled with VGLUT2, 96% of these double-labeled Cu terminals were in the GCD; 86% of all Cu MFs colabeled with VGLUT2, 43% of all Cu SBs colabeled with VGLUT2. B: Percentage of Sp5 terminal endings colabeled or not colabeled with VGLUT2. 25% of all Sp5 terminals colabeled with VGLUT2, 83% of these doubled-labeled Sp5 terminals were in the GCD; 85% of all Sp5 MFs colabeled with VGLUT2, whereas 18% of all Sp5 SBs colabeled with VGLUT2.

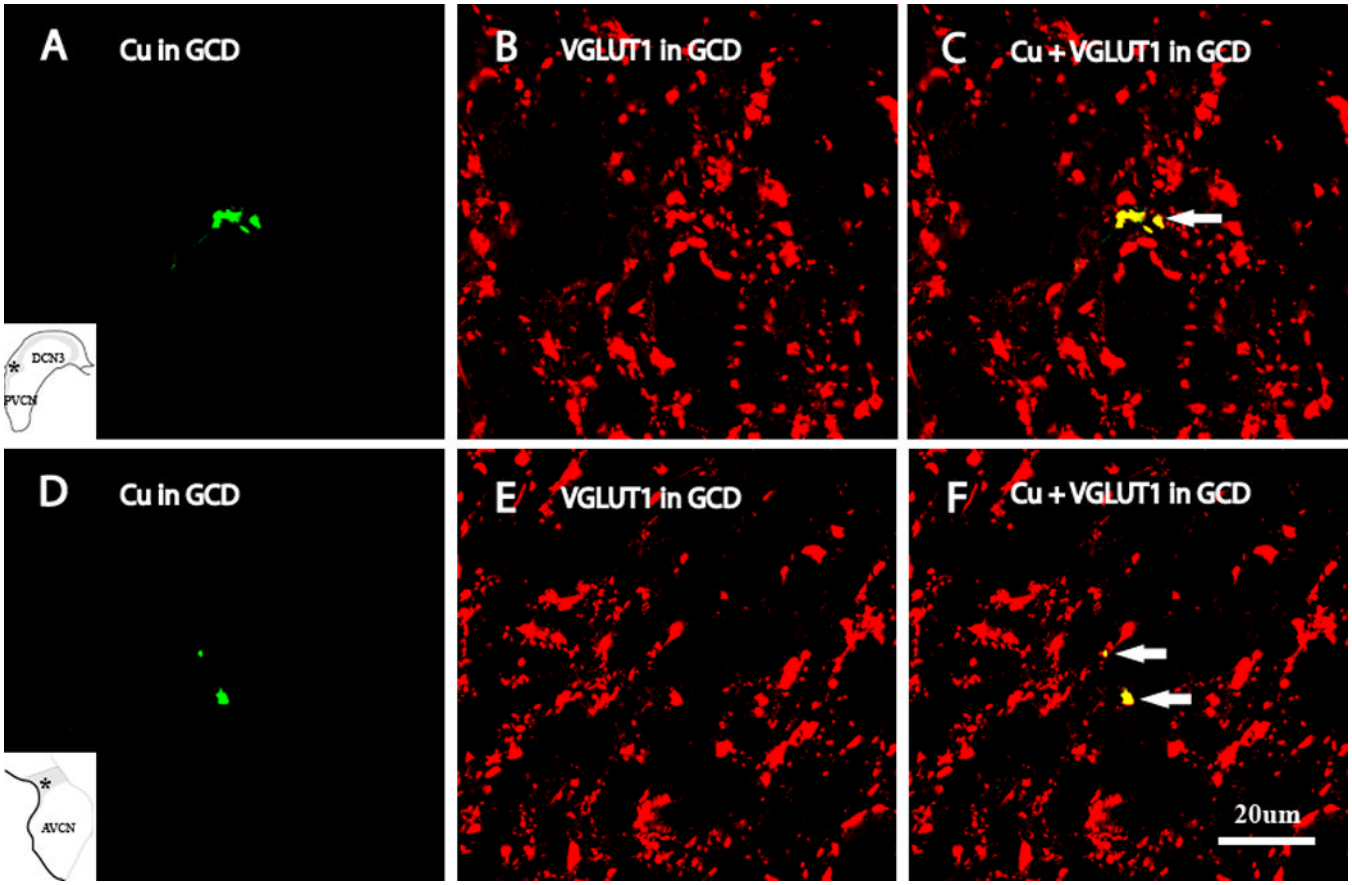

Figure 8.

High-magnification confocal images (×100) showing colocalization of anterogradely-labeled Cu terminal endings with VGLUT1 in different regions of the GCD as designated by insets. Green, BDA-labeled Cu terminals; Red, VGLUT1; Yellow, double-labeled terminals. Colocalization of VGLUT1 with a Cu MF in GCD is shown by arrow in C. Colocalization of VGLUT1 with a Cu MF and SBs in GCD are shown by arrows in F.

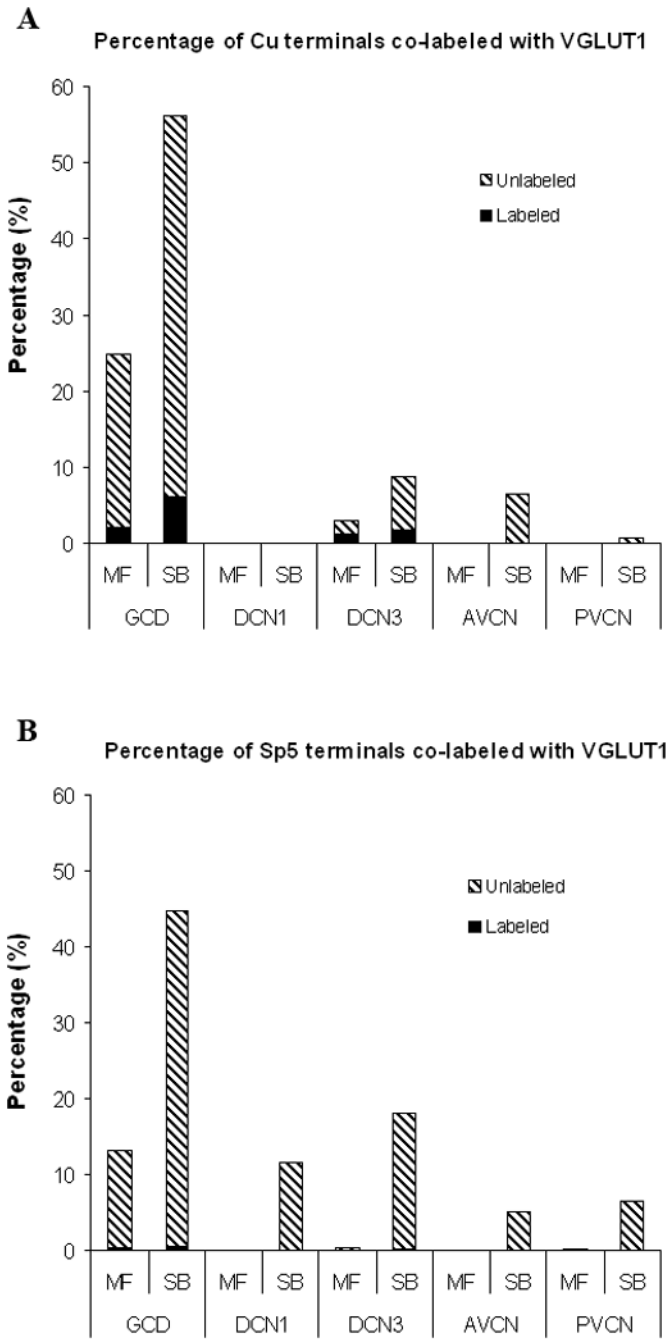

Figure 9.

Percentages of labeled Cu and Sp5 terminal endings colocalized with VGLUT1 in different subdivisions of the CN (Cu, n=2; Sp5, n=2). A: Percentage of Cu terminal endings colabeled with VGLUT1. 11% of all Cu terminals colabeled with VGLUT1, all double-labeled Cu terminals were found in the GCD and DCN3. B: Percentage of Sp5 terminal endings colabeled with VGLUT1. Only 1% of all Sp5 terminals colabeled with VGLUT1. All double-labeled Sp5 terminals were found in the GCD and DCN3.